Multiscale modeling of droplet interface bilayer membrane networks

Eric C. Freeman,[1,a)] Amir B. Farimani,[2] Narayana R. Aluru,[2] and Michael K. Philen[3]
[1]*College of Engineering, University of Georgia, Athens, Georgia 30602, USA*
[2]*Department of Mechanical Science and Engineering, Beckman Institute for Advanced Science and Technology, University of Illinois at Urbana-Champaign, Urbana, Illinois 61801, USA*
[3]*Department of Aerospace and Ocean Engineering, Virginia Tech, Blacksburg, Virginia 24061, USA*

(Received 31 August 2015; accepted 28 October 2015; published online 9 November 2015)

Droplet interface bilayer (DIB) networks are considered for the development of stimuli-responsive membrane-based materials inspired by cellular mechanics. These DIB networks are often modeled as combinations of electrical circuit analogues, creating complex networks of capacitors and resistors that mimic the biomolecular structures. These empirical models are capable of replicating data from electrophysiology experiments, but these models do not accurately capture the underlying physical phenomena and consequently do not allow for simulations of material functionalities beyond the voltage-clamp or current-clamp conditions. The work presented here provides a more robust description of DIB network behavior through the development of a hierarchical multiscale model, recognizing that the macroscopic network properties are functions of their underlying molecular structure. The result of this research is a modeling methodology based on controlled exchanges across the interfaces of neighboring droplets. This methodology is validated against experimental data, and an extension case is provided to demonstrate possible future applications of droplet interface bilayer networks. © *2015 AIP Publishing LLC*. [http://dx.doi.org/10.1063/1.4935382]

I. INTRODUCTION

In the search for new biologically inspired materials, one topic of interest is the potential of a material based on cellular mechanics, using the controlled transport of charged ions within a fluidic network for various applications.[1] The primary inspiration for this material is the capability of cellular systems to collectively demonstrate abilities such as voltage generation,[2,3] cell-to-cell signaling,[4] and complex decision making processes.[5] Each of these desired abilities requires the integrated response of multiple units working in parallel towards a common goal. Therefore, this proposed cellular-mimicking material must effectively combine multiple units in large interconnected arrays to best mimic natural cellular systems.

The droplet interface bilayer (DIB) technique[6,7] is selected for this purpose. DIBs, developed originally by Bayley *et al.*[6–8] and Funakoshi *et al.*[9] and developed further by Ces and co-workers[10,11] and Sarles and co-workers,[12–15] have been considered for use as autonomous materials, or stimuli-responsive materials that are capable of independently reacting to changes in their environments. In this approach, liposome-laden aqueous droplets are deposited into oil reservoirs, wherein the contained liposomes migrate to the oil-water interface, spreading into ordered lipid monolayers on the droplet surfaces. Manipulating these lipid-coated droplets into contact creates interfacial lipid bilayer membranes which approximate natural cellular membranes (Figure 1).

[a)]ecfreema@uga.edu

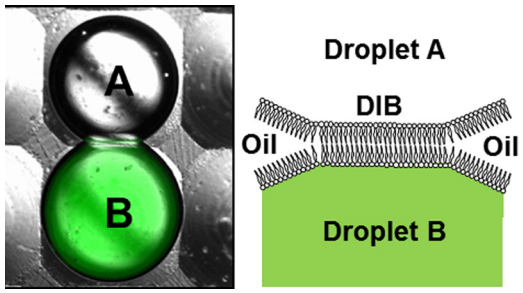

FIG. 1. Droplet interface bilayers. Phospholipids are used as an organic surfactant, creating ordered lipid monolayers at oil-water interfaces. Manipulation of these droplets into contact creates interfacial lipid bilayers.

The result is a collection of membranes at the droplet-droplet interfaces that divide the material into collections of isolated aqueous subcompartments.

Unmodified interfacial lipid bilayer membranes are highly impermeable to ions, but they may be modified through the incorporation stimuli-responsive biomolecules such as voltage-gated channels, allowing for controlled, selective exchanges between neighboring droplets. Typically, these biomolecules fall into two categories—passive and active. Passive channels allow for transport that follows the electrochemical energy gradient, such as the passive diffusion of ions from a high concentration to a lower concentration. Active proteins, such as bacteriorhodopsin, are able to actively shape the droplet contents through powered transport, generating concentration gradients and charged membranes. These changes in the droplet contents may then be used to communicate the status of the droplet and pass messages through actions similar to action potential generation, demonstrating a collective response within droplet networks.[16] These droplet networks may be assembled in increasingly complex configurations, advancing gradually towards the tissue scale.[8]

These systems have traditionally been examined through voltage-clamp methods. An electrical input is supplied by silver/silver-chloride (Ag/AgCl) electrodes piercing the droplets, activating embedded channels and pores. Consequently, electrical circuit models have been the primary method for predicting the system behavior, approximating the material as a series of capacitors and resistors.[17,18] These models have worked well for replicating experimental data and illustrating the electrical properties of the DIB networks; however, further modeling efforts are necessary to better characterize the systems.

II. METHODOLOGY

A three-tiered multiscale model outlined in Figure 2 is proposed. This model begins at the atomistic level for simulating the embedded biomolecules within the membrane, focusing primarily on passive biomolecules. Data and equations for the channel behavior are then combined with results from continuum electrostatics model designed to address limitations of the

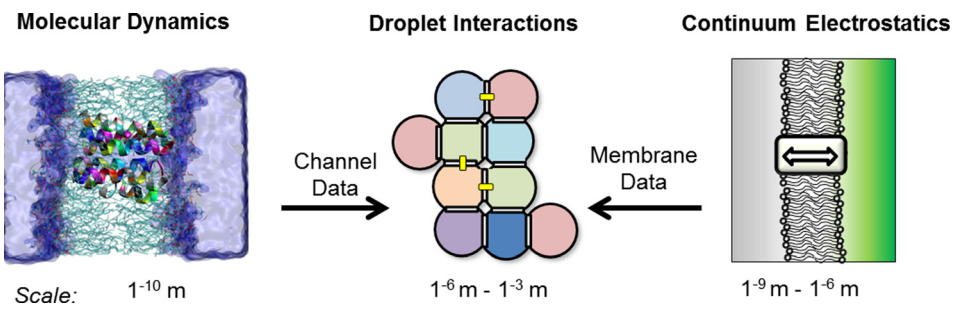

FIG. 2. The proposed hierarchical multiscale model. Molecular dynamics will be employed to assess the conductivity and mechanics of the embedded transport biomolecules and combined with continuum electrostatics for the assessment of the membranes. Findings from the previous two models are used to develop a functional network model.

atomistic model. The membrane and channel data are then injected into a droplet-interactions model for simulating DIB network behaviors. This approach links the observed macroscopic behaviors of the DIB network (such as voltage and current) to the underlying structure and composition of the material.

A. Molecular dynamics model

The first length scale of interest examines the transport biomolecules embedded in the DIB membranes. These complex biomolecules govern transport across the membrane and respond to multiple stimuli ranging from transmembrane potential to physical force.[19–22] Modeling these biomolecules is best accomplished through molecular dynamics (MD) simulations due to the complexity of the biomolecular structures. MD simulations of the voltage-gated channel formed by the polypeptide Alamethicin (Alm) channel are presented here as an example of this approach. Alm is a passive voltage-gated biomolecule that allows for the flow of ions along their chemical energy gradient between droplets.

Polypeptides bound to lipid bilayer play a significant role in transmembrane signal transduction and cellular mobility.[23,24] In recent years, a wealth of knowledge was added to literature about polypeptides that form pores in membranes;[24–27] however, it is a difficult area of study because unlike the transmembrane proteins there is no access to crystallography data of polypeptide channels inside the membranes.[28,29] Among all polypeptides channels, the most studied channel-forming peptide is Alamethicin.[30–33] Some studies have already shown the gating behavior of Alm channel and its I-V curve,[24,27,34–36] however, the fundamental insight into the mechanism of gating at molecular level is still unclear. This is rectified by examining the pore diameter as a function of the applied electrical field.

To study the Alamethecin (Alm) channel formation and water/ion conductance through the channel, extensive molecular dynamic simulation using GROMACS 4.5.5 (Ref. 37) were conducted. The CHARMM 27 standard force field was used combined with the TIP3P water model to simulate the interaction between ions, water, and Alm peptide.[38] The simulation temperature is kept constant and is equal to T = 295 K during the whole simulations using Nosé-Hoover thermostat.[39] Initially, the Alm helices were placed with the radius of 0.8 nm inside a patch of lipid bilayer (POPC) with 5 nm × 5 nm dimensions. Simulations were performed for two cases of 5 helices (16729 atoms) and 6 helices (16893 atoms, Figure 3(a)). After around 80 ns, the transmembrane water channel is formed (Figure 3(b)). To find the equilibrated channel radius, the HOLE program[40] was used, providing the initial pore radius in Figure 3(c).

The external electric fields are reported in terms of a transmembrane voltage difference $V = EL_z$, where E is the electric field strength and L_z is the length of the simulation system in the z direction.[41] The time-dependent ionic current $I(t)$ was measured, by using the definition of current, $I = dq/dt$ or

$$I(t) = \frac{1}{L_z}\sum_{i=1}^{n} q_i \left[\frac{z_i(t+\delta t) - z_i(t)}{\delta t}\right], \tag{1}$$

where the summation is for all the ions, δt is chosen to be 5 ps, z_i and q_i are the z-coordinate and charge of ion i, and n is the total number of ions, respectively. The ionic current data are averaged for 20 ns of simulation for each applied bias. Biases ranging from −120.0 to 120.0 mV in axial (transmembrane) direction were applied. Through computing the ionic current, the I-V curve of Alm channel has been generated. For each applied bias, the 80 ns-equilibrated structure of 6 Alm channel was used.

The Alm(6) bundle I-V curve shows that gating occurs at ∼±70 mV (Figures 3(c) and 3(d)). The I-V curve passes through the origin and is symmetric about it. The conformational changes of Alm helices (radius of channel) with different applied biases (Figure 3(c)) were computed to understand the gating mechanism of the Alm channels. The constriction regions (constrictions #1 and #2) of Alm channels are designated in Figure 3(c). The radii of channel at biases = 0, 25, and 50 mV show that the constriction region #1 is mostly intact and constriction

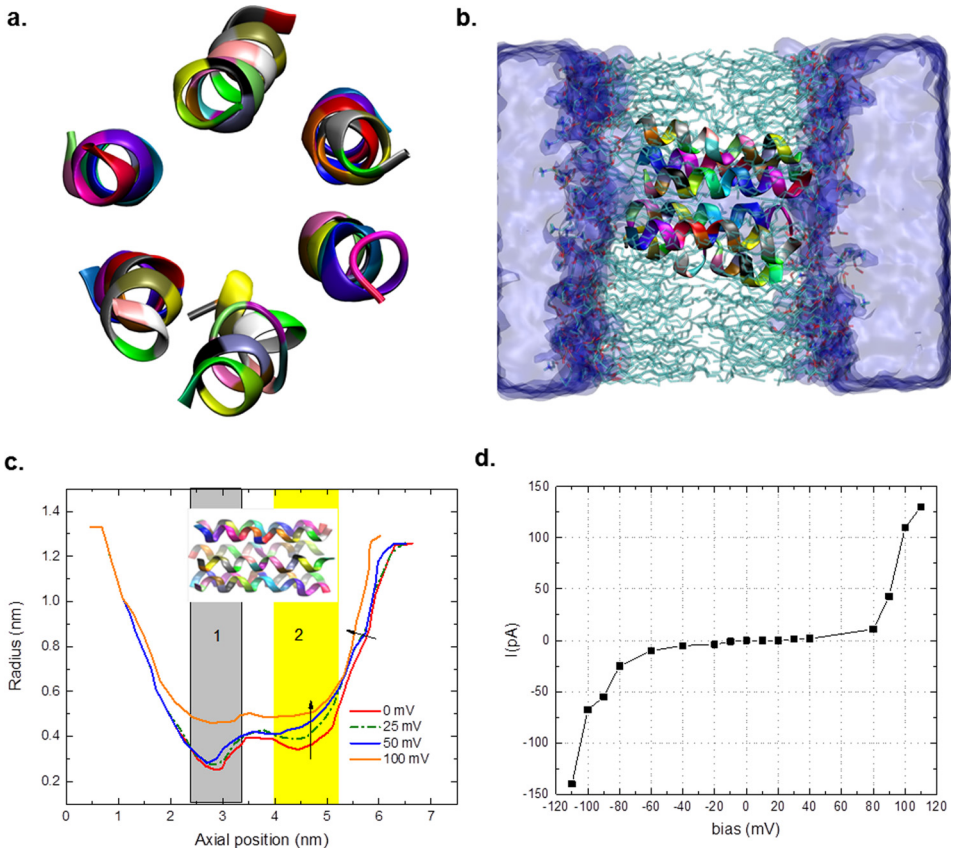

FIG. 3. Molecular dynamics analysis of the alamethicin polypeptide. (a) Front view of 6 helixes configurations after equilibration within the membrane (only Alm is shown). The center of the ring creates a conductive pore that allows for transport across a lipid membrane. (b) Side view of the 6 helixes configuration within the membrane showing water permeation, demonstrating how alamethicin creates conductive pore that spans the membrane. (c) The changes in the radius of channel versus different applied biases, demonstrating gating at higher bias potentials and increasing the pore conductivity. (d) I-V curve of 6 Alm helices channel at different voltages.

region #2 is gradually expanding. At 100 mV, the constriction region #1 opens suddenly, allowing for gating. It is worth noting that the Alm channel did not gate while only one constriction region is open. A channel radius of >0.5 nm in the constriction region is required for the passage of ions and gating of the channels. (The maximum radius of an ion is 0.21 nm and it requires to be hydrated with at least 3 water molecules.) By reversing the direction of applied bias, the role of constriction regions is interchanged. The electrostatic forces exerted on the Alm internal lining residues due to the applied bias and the indirect axial forces originated from electro osmosis flow give rise to the opening of the constriction regions. From this, one concludes that constriction region #2 opens with lower bias compared to constriction region #1.

The computed Alm(6) bundle I-V curve shows symmetric gating. This contradicts observed experimental results,[42] where the gating is uni-directional dependent on the direction of Alm insertion. In the simulations, the insertion of Alm inside the membrane is handled through equilibration[27] and does not capture the insertion of the peptides and subsequent assembly into pores, as this process takes much longer than currently feasible with molecular dynamics. To rectify this gap between the model and experiment, Alm is assigned directionality dependent on the direction of insertion from the bulk into the membrane in other portions of the model.

B. Continuum electrostatics model

Current computing resources limit the practicality of atomistic simulations at the mesoscale, necessitating the use of continuum electrostatics methods. Membrane processes are first

modeled through continuum electrostatics, and these results are combined with the atomistic results for the final model. The continuum electrostatics model recognizes that the continuous redistribution of charged ions is largely responsible for the experimentally observed results, and focuses on providing a tractable methodology for studying these phenomena.

The interactions between the charged ions in solution and the developed transmembrane potentials may be described through the Poisson equation (Equation (2)), linking the development of the electrostatic potentials φ to changes in a continuous description of the polarization ρ and the dielectric permittivity ε. The permittivity in the droplets is assumed to match the bulk permittivity of water, as the droplet radius typically does not drop below 10 μm, eliminating constriction effects on the permittivity.[43] This electrostatics model approximates the charged ions as a continuum of excess charge or polarization rather than tracking their individual trajectories

$$\nabla \cdot \varepsilon \nabla \varphi = -\rho. \tag{2}$$

Assuming negligible convection in the fluid, the flux of ions in the solution is determined by a combination of electrical migration $uzFcd\varphi/dx$ and chemical diffusion Ddc/dx. Here, J is the ion flux, u is the ion mobility, z is the valence charge, F is Faraday's constant, c is the ion concentration, and D is the diffusion coefficient

$$\sum J = u_i z_i F c_i \frac{d\varphi}{dx} + D_i \frac{dC}{dx}. \tag{3}$$

When the net flux is zero at equilibrium, ($\sum J = 0$) these combined fluxes allow for the derivation of the classic Boltzmann distribution. Combining this with the Poisson equation (Equation (2)) produces the Poisson-Boltzmann distribution, appropriate for systems operating near or at an equilibrium.[44] This description is suitable for our purposes as the electrical currents are minimized by the impedance of the lipid membranes. Equation (4) is the Poisson-Boltzmann distribution for a combination of free ions in solution and fixed lipid charges ρ_{fixed}. Here, R is the gas constant and T is the absolute temperature

$$\nabla \cdot \varepsilon \nabla \varphi = -\sum z_i F c_{bulk,i} \exp\left(\frac{-z_i F \varphi}{RT}\right) - \rho_{fixed}. \tag{4}$$

The solution of these equations with various simplifications[45] allows for the derivation of the electrical circuit analogues as functions of the droplet states, including conductivity, capacitance, and chemical and electrical potentials. This approach links the observed electrical quantities and the resulting material polarization and transport, providing an electrical approximation of the membranes based on their structure and properties.

C. Droplet interactions model

A cumulative network model is developed from the two previous models, employing a droplet-droplet interaction framework. Each droplet is defined as an entity described by a series of values such as volume, ionic concentrations, transport biomolecules, and electrostatic potentials. Differences between neighboring droplets influence their interfacial exchange of contents and charge, gradually altering the droplet composition. The droplet interactions model is combined with the electrical circuit model,[17] linking the observed electrical properties with ion migration and accumulation/depletion. A summary of the model may be seen in Figure 4.

1. Droplet model electrical components

Ion species in the system are assigned a valence charge z, bulk diffusion coefficient D_{bulk}, membrane diffusion coefficient D_{blm}, and respective droplet molar concentrations c_i. Bulk diffusion coefficients are taken from experimental studies by Samson *et al.*[46] Cation diffusion is generally lower than anion diffusion across the membrane[47] due to the positive interior dipole

potential of the lipid membranes.[48] Since calculated values for individual ion permeabilities through the selected 1,2-diphytanoyl-sn-glycero-3-phosphocholine (DPhPC) membranes are not available in the literature, a net conductance level will be used from experimental conductivity measurements[49] with cationic conductivity set to half that of the anionic conductivity.

The exchange across the membranes is dependent on the electrostatic potential φ_{elec} and chemical potential φ_{chem}, capturing the competing migration and diffusion forces exerted on the ions in the solution (Equation (3)). Equation (5) is combined with the four-node KCL stencil for the membrane (Figure 4),[17,49] and the transmembrane potentials are calculated as the difference in electrostatic potential between the nodes at either side of the membrane ($\Delta\varphi_{elec}$). The conductance G_{bulk} of the droplet interiors are updated according to the internal state of the droplets (Equation (7)), and the chemical concentration gradients are allowed to drive diffusion events across the system through Equation (8)

$$C_{blm}\frac{d\Delta\varphi_{elec}}{dt}+\frac{dC}{dt}\Delta\varphi_{elec}+G_{blm}(\Delta\varphi_{elec}+\varphi_{chem})=0, \tag{5}$$

$$i_{transport}=\sum G_i(\varphi_{elec}+\varphi_{chem}), \tag{6}$$

$$G_{bulk}=\frac{F^2}{RT}\sum D_{bulk,i}c_i, \tag{7}$$

$$\varphi_{chem}=\frac{k_bT}{ze}\ln\left(\frac{c_{i,1}}{c_{i,2}}\right), \tag{8}$$

$$\frac{dc_{i,j}}{dt}=\frac{1}{F}\frac{i_{transport,i}}{Vol_j}. \tag{9}$$

The linear relationship between the conductance and the ionic concentrations (Equation (7)) is valid for conditions with low voltages and low currents, assuming that the voltage is below the electroporation threshold, and assuming ion depletion in the double layers at the interfaces does not occur.[45] All of these assumptions are reasonable for a DIB network.

2. Droplet model mechanical components

Ionic accumulations and depletions trigger additional actions such as osmotic swelling. While this swelling may be useful for actuation purposes,[50] it is often destructive, rupturing the

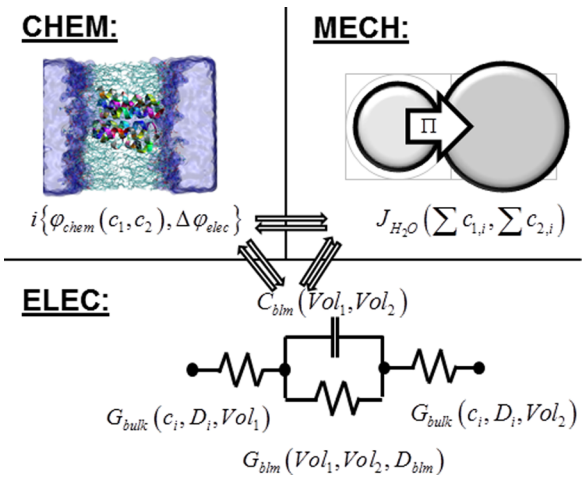

FIG. 4. The droplet interactions model. All interactions are classified as mechanical, chemical, and electrical, each with their own set of equations. The model is then applied to large DIB networks with various transduction pathways.

interfacial membranes, and contributing to droplet coalescence.[51] The osmotic swelling $dVol_{droplet}$ of each droplet is calculated as the summation of the osmotic flux across each of the droplet's interfacial membranes. This is a function of the membrane hydraulic diffusivity K_{blm}, membrane area A_{blm}, existing hydrostatic pressure across the membrane due to varying droplet sizes ΔP_{blm},[52] and osmotic pressure π. The osmotic pressure is calculated through a summation of the difference in bulk ion concentrations on either side of the membrane and their respective osmotic coefficients θ (assumed to be unity here). The diffusivity K_{blm} is adapted from studies by Negret *et al.*[53]

$$\frac{dVol_{droplet}}{dt} = \sum_{i}^{n_{droplet}} \left[K_{blm,i} A_{blm,i} \left(\sum_{j}^{n_{ion}} \pi_j - \Delta P_{blm,i} \right) \right], \tag{10}$$

$$\pi_j = RT\theta(c_{j,i} - c_{j,e}). \tag{11}$$

3. Droplet model chemical components

The behavior of the transport biomolecules must be reduced to a more compact thermodynamic form for the droplet-droplet model while still retaining pertinent MD information such as conductivity and gating behavior. This requires an approach similar to the one developed by Endresen *et al.*,[54] calculating the rate of transport across the biomolecules through energetic balances equating the work done by the protein to the work required to transport an ion across the membrane[55] (Equation (12))

$$e\varphi_{protein} = ze(\varphi_{elec} + \varphi_{chem}). \tag{12}$$

These equations must take into account multiple gating behaviors such as voltage, ligand, and tension activation modes. This is accomplished by modifying the overall current through the biomolecule by a gating probability x_{open}, which calculates the likelihood of gating based on comparing the activation threshold to the current condition. For a voltage-activated channel such as Alm, this may be written as[54]

$$x_{open} = \frac{1}{2}\left[1 + \tanh\left(\frac{q_{gate} e(\varphi_{elec} - \varphi_{activate})}{k_b T}\right)\right]. \tag{13}$$

The resulting equations for current across a transport biomolecule i_{bio} may be written in a general form as seen in Equation (14), multiplying the open-state conductance of the biomolecule G_{bio} by the gating probability x_{open} predicted by Equation (13) and some function of the transmembrane state f. The function f is selected dependent on the available information—for the Alm simulation presented in the following chapter; the function is simplified to a transmembrane potential dependent conductivity to best fit the data available from the simulations where $i_{bio} = G_{bio}(\varphi_{elec})(\varphi_{elec} + \varphi_{chem} + \varphi_{protein})$

$$i_{bio} = G_{bio} x_{open} f\left(\frac{e(\varphi_{elec} + \varphi_{chem} + \varphi_{protein})}{2k_b T}\right). \tag{14}$$

4. Solution methodology

A python script was developed to automatically generate the previous interaction equations. Droplets are assembled into networks, and biomolecules are assigned to the shared interfacial bilayers. Ion transport across the droplet chains is handled through a series of linked electrical circuit equations, updating the internal values through Equations (6) and (7). Each droplet is assigned multiple nodes at the connective bilayers, and the appropriate connections are made with resistor and capacitor elements (Equation (5), Figure 4). The generated equations provide

a large stiff system of differential algebraic equations (DAEs) which are solved using the IDAS solver available from Lawrence Livermore[56] through the CasaDI shell.[57] The end result is a model of droplet-droplet interactions, where the internal properties of each droplet dictate the communications across the interfacial membranes.

III. RESULTS AND DISCUSSION

A. Model validation

The full multiscale approach is validated by simulating a DIB network with Alm channels and comparing to experimental results. Three droplets all containing the Alm biomolecules (5 μg/ml) were deposited in a crate substrate in a linear chain (Figure 5(a)), allowing for a bi-directional path of Alm channels between the source and ground. Since Alm is present in each droplet in the network, the Alm channels were inserted in both directions in both membranes. A 100 mV 1 Hz sinusoidal voltage was created between the electrodes. At this frequency, the potential evenly distributes across the two membranes (similar to a voltage divider),[17] allowing for initial transmembrane potentials of 50 mV assuming uniform membrane qualities. This level of transmembrane potential is insufficient to activate the Alm channels as shown in Figures 3(c) and 3(d), and the measured current is primarily a capacitive response to the changing transmembrane potentials, where $i = C_{blm}\frac{d\varphi_{elec}}{dt}$. A 50 mV DC transmembrane potential is then combined with the original oscillating potential, and spikes are observed for positive potentials as the redistributed transmembrane potential reaches 75 mV at their peaks (Figure 5(e)). The experimental data were imported into python scripts for analysis, and the current for 40 voltage cycles was averaged for comparison with the model predictions (Figure 5(e)), smoothing the individual gating events.

The Alm channels are modeled with two conductance states observed in the MD simulations (Figure 5(d)). While Alm exhibits additional gating states,[49] these higher states are not included as the required membrane potential may cause undesired membrane rupture (≈100 mV)

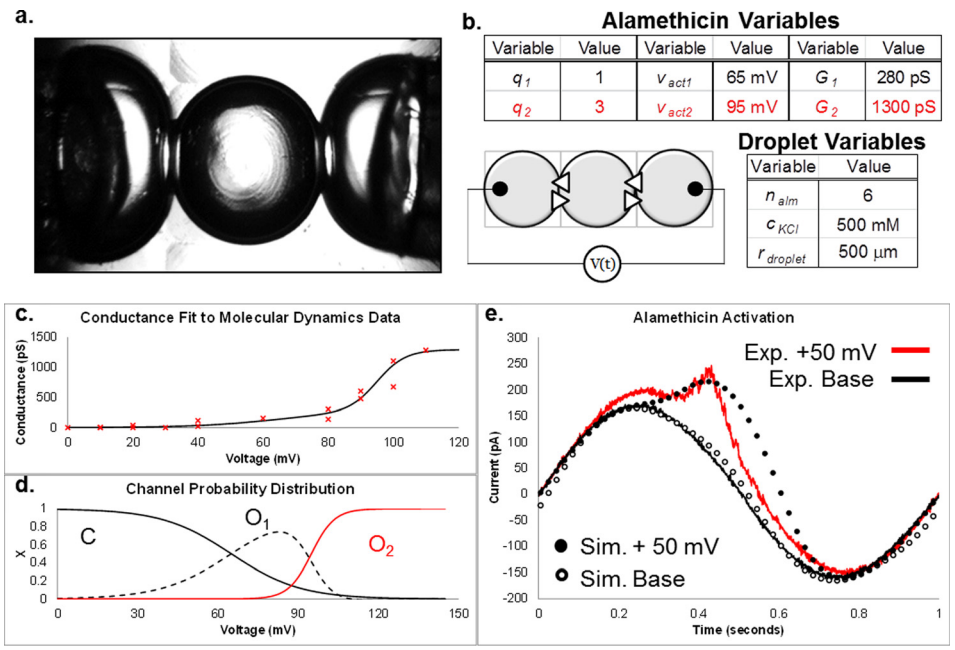

FIG. 5. Multiscale model validation through a simple DIB network with Alm channels. (a) Three droplets containing dissolved Alm biomolecules are deposited in an oil reservoir with electrodes embedded within the bordering droplets. A 100 mV sinusoidal voltage is supplied between the electrodes across the two membranes both with and without a 50 mV DC offset, and the results for 40 cycles are averaged and plotted in (d). This simple three-droplet network is recreated using the inputs from (b) and equations fit to the molecular dynamics simulation data in (c) and (d), and the predicted results are compared to the experimental results in (d).

$$C \leftrightarrow O_1 \leftrightarrow O_2. \tag{15}$$

Equation (13) is modified to accommodate the multiple gating stages, and the channels are assumed to follow the progression depicted in Equation (15), progressing from closed pores through the two open conductance states. The resulting fit for these conductance states to the MD data for a single channel may be seen in Figures 5(c) and 5(d). The ionic conductance of Alm was calculated by dividing the current by the simulated voltage from Figure 3(d), and the gating charges and thresholds were varied until a suitable match was found.

Alm exhibits some selectivity in its conductance.[58] This is not considered here, as this primarily influences the ion concentrations within the droplets (Equation (9)), which in turn influences the Nernst potentials (Equation (8)). Here, the droplets are large (1 mm diameter), and any shifts in their compositions will take a long enough time to be considered negligible over the course of the presented experiments. This is shown in Figure 7(c) as well.

The three droplet chain containing bi-directional Alm channels was recreated in the model as seen in Figures 5(b)–5(e) and subjected to the same applied potentials. The predicted output current matches the experimental current, exhibiting the predicted two stage gating process from Equation (15), with a brief spike in conductivity at the peak voltages (Figure 5(e)). This current does not follow typical Alm conductivity sweeps, as the current contains capacitive and conductive elements to test the predictions of the model. A sinusoidal voltage sweep provides the underlying phase-shifted sinusoidal capacitive current, and increasing the DC component of the command signal generates the conductive spikes due to Alm gating.

B. Model extension example

With the model validation complete, a theoretical DIB network with selective ionic pathways is constructed within the model to demonstrate the underlying links between the measured electrical signals and the changes in droplet compositions. Here, theoretical ion-selective voltage-gated channels (representative of those commonly found in plant cells) are created and simulated, including K^+, Na^+, Ca^{2+}, and Cl^- selective channels (Figure 6). Droplets containing these channels are arranged into a network designed for sorting cations from a high-concentration source droplet to their respective storage droplets. The channels are originally dissolved within the droplets, and it is assumed that these channels distribute themselves evenly across the membranes connected to their respective droplets, resulting in a similar channels-per-membrane value for each membrane. Three base channel solutions are included as shown in Figure 6, with the tri-color droplet assuming an equal blend of the first three. Each solution contains a selective channel, and these channels are assumed to populate the membranes connected to each droplet. A voltage is applied across the interfacial membranes, and the embedded selective channels facilitate the transport of ions along their respective pathways to the ground electrodes.

Initial results are summarized in Figure 7. As expected, the simulated ions respond to the applied potential (Figure 7(a)), moving from droplet to droplet along their respective chains (Figure 7(b)). Several competing effects are observed. The transport is initially aided by the chemical potentials (Equation (8)), but this gradually reverses and inhibits the transport across each membrane until equilibrium is reached. At this point, the generated chemical potential balances the supplied electrical potential. Osmotic swelling is also accounted for (Equation (10)), gradually reducing the chemical potentials through the flux of water across the membranes.

This osmotic behaviour is ultimately beneficial if the overall efficiency is defined as the total number of moles in the storage droplets divided by the total number of moles in the network, reducing the chemical energy necessary for ion transport. At first glance, this contrasts previous observations in which the osmotic diffusion reduced the efficiency of the chemical-electrical energy conversion;[2] however, the overall mechanic remains unchanged. Osmotic flux continuously reduces the stored chemical energy in the network, allowing for continued transport when a surplus electrical energy is provided.

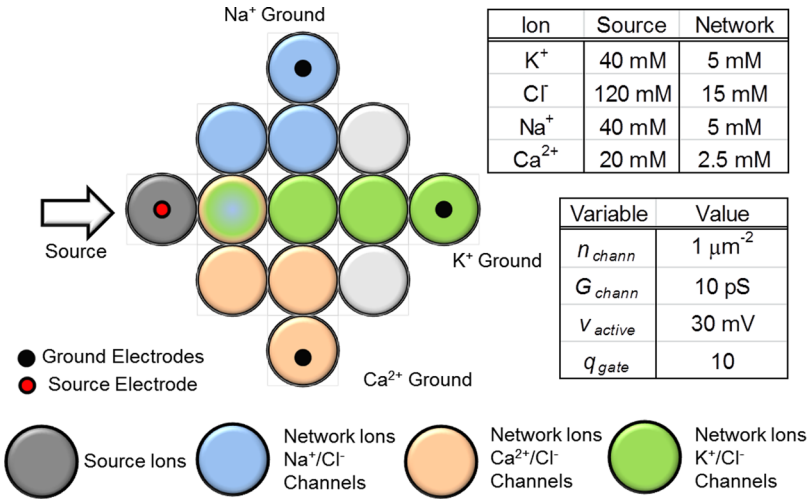

Ion	Source	Network
K^+	40 mM	5 mM
Cl^-	120 mM	15 mM
Na^+	40 mM	5 mM
Ca^{2+}	20 mM	2.5 mM

Variable	Value
n_{chann}	1 μm^{-2}
G_{chann}	10 pS
V_{active}	30 mV
q_{gate}	10

FIG. 6. Ion sorting example using selective pathways. A simple network is created with three pathways for sodium, calcium, and potassium transport. In keeping with the method of manufacture for DIB networks, three solutions containing different theoretical selective channels are simulated. As these droplets are connected into the networks, the channels included within each droplet will spontaneously insert themselves into the surrounding membranes. The tri-color droplet contains all three theoretical selective channels, and the dark grey droplet contains the elevated concentrations of ions that will be redistributed along their respective pathways in the network.

The surface area–volume ratio intuitively dictates the characteristic time required for equilibrium (Figure 7(c)). The transport is limited by the channel conductivity (scaled by area, Figure 6), and the transport equilibrium is limited by the chemical potentials, linked to the

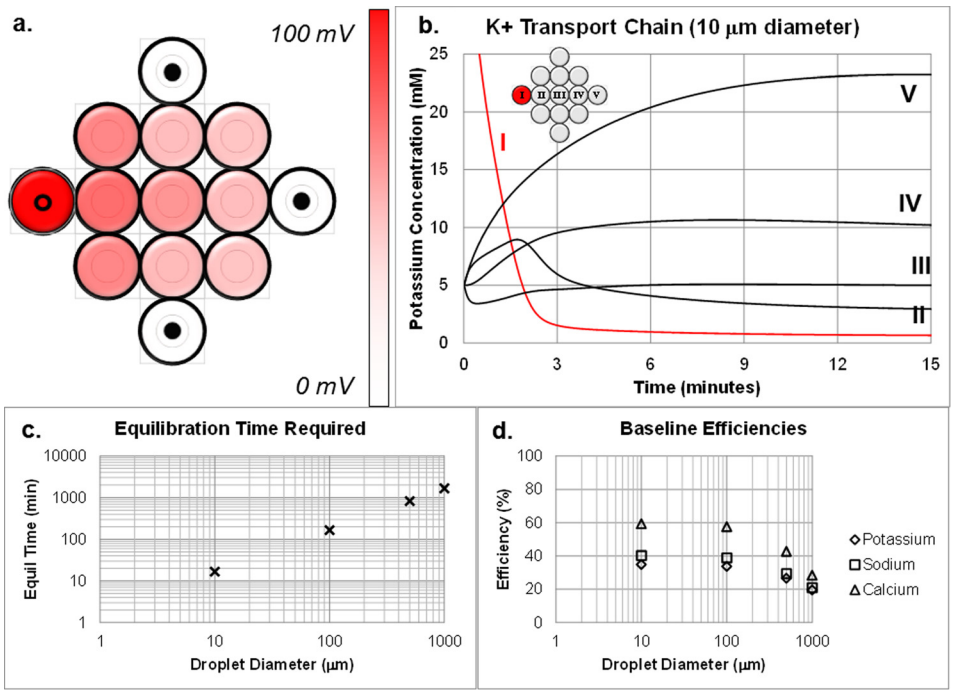

FIG. 7. (a) An applied voltage distributes itself evenly across the network, generating membrane potentials and activating the embedded channels. (b) A traveling wave of cations move across the droplets with the voltage—here, the potassium concentration is plotted with respect to time in each droplet. The transport in the sodium and calcium channels is similar. (d) As the size of the droplets increases, the time required for equilibration (steady-state ion concentrations) increases linearly with the droplet diameter. (d) Efficiency is defined as the number of selected ions in the terminal droplet divided by the total ions in the network. This efficiency is decreased as the droplet size increases.

droplet volume. The efficiency of each cation transport chain at varying geometries is plotted in Figure 7(d). With larger droplets the overall efficiency is reduced, but the relations between the respective cations are preserved. Ca^{2+} transport is the most efficient, linked to lower concentrations and higher valence charge. A deviation between the K^+ and Na^+ transport efficiencies is also observed due to competition between the Ca^{2+} (top) and K^+ (middle), which vanishes when the transport is fixed along their respective pathways rather than bleeding into adjacent droplets through unwanted channel insertion. Here, the channels are fixed into their respective pathways, rather than allowed to insert uniformly into all neighboring membranes.

IV. DISCUSSION

The primary point of emphasis for this model was the transport of charged ions between adjacent droplets, and the ability to alter or evolve the macroscopic properties of the DIB networks through these transport processes. This improves existing DIB modeling methodologies by linking the measured current and voltage data recorded during experiments to the underlying physical mechanisms responsible. The primary benefit from this approach is that the droplet networks may now be simulated with or without embedded electrodes. The electrodes commonly present in the experimental and theoretical discussions do provide a convenient source of energy for driving the material response, but this model now allows the simulation of DIB networks using chemical energy[2] or photosynthetic energy harvesting[7] sources for material activation and response, removing the previous modeling limitations that required clearly defined source and ground droplets within the material.

The end result is a step forward for modeling the DIB material concept. Currently, the majority of the published work focuses on membrane transport with a supplied voltage, but the cellularly inspired material is capable of functioning outside of the laboratory for applications such as mechanosensing,[13] energy harvesting,[59,60] and osmotic actuation.[8,61] These applications require a new methodology for material modeling that accurately captures the exchange between the constitutive droplets within the DIB networks, which has been successfully developed here.

V. CONCLUSION

Cellularly inspired materials are created through complex networks of biomimetic stimuli-responsive membranes separating aqueous droplet compartments through the droplet interface bilayer technique. These networks are often modeled empirically, approximating the material as a combination of capacitors and resistors. This modeling methodology has proved suitable for simulating experimental voltage-clamp results; however, these models restrict possible DIB mechanics such as osmotic actuation and chemical energy conversion.

The modeling methodology presented here develops a multiscale and multiphysics model for predicting the performance of complex networks of droplet interface bilayer membranes. The hierarchical multiscale modeling scheme developed in this work is an appropriate method for simulating these advanced applications of the cellularly inspired material and aids in illustrating the potential of the cellularly inspired material.

This model was validated against experimental results. The results were presented as traditional current-voltage relationships appropriate for the experimental design; however, the model also takes into account underlying ion concentration shifts and exchanges between the droplets. The model was then extended to an ion-sorting case employing selective channels, showing how an applied electrical stimulus may be translated into changes in the droplet chemical compositions if the characteristic droplet dimensions are reduced. The revised model allows for the incorporation of chemical and mechanical inputs in addition to the standard electrical inputs, and the modeling methodology seen here will be useful for simulating DIB network behavior outside of the laboratory.

ACKNOWLEDGMENTS

The authors graciously acknowledge the funding support of NSF MCB Grant No. 1244014 and AFOSR BRI Grant No. FA9550-12-1-0464.

APPENDIX: EXPERIMENTAL

Networks of droplet interface bilayers[6] were constructed using a machined acrylic-glass egg-crate substrate, allowing the droplets to settle into predefined locations and form fluidic networks at their points of contact.[7] The substrate was CNC machined from acrylic glass (Optix, Plaskolite), selected for its translucency and hydrophobicity. The crate substrate consists of two portions, an oil well and a network of smaller individual crates. The liposome-containing solution was created with a 500 mM KCl solution (Sigma Aldrich), 10 mM MOPS (Sigma Aldrich), and 2 mg/ml DPhPC (Avanti Polar Lipids). The liposomes were extruded through 0.1 μm filters to ensure uniform liposome size using the Avanti extrusion kit. These liposome-containing droplets were placed in a hexadecane oil bath (Sigma Aldrich) the crate substrate and allowed to rest separately for 3–5 min for the proper formation of lipid monolayers at the water-oil interface. These droplets were then brought into contact through micromanipulators (Siskiyou, Burleigh), and DIB networks were formed.

Alamethicin (Alm) was purchased from Cayman Chemicals and dissolved in ethanol (Sigma Aldrich) at 1 mg/ml. When droplets with the Alm biomolecules were required, 5 μl of the ethanol-Alm solution was added directly to 1 ml of the buffer solution containing dissolved phospholipids, resulting in a concentration of 5 μg/ml Alm in the lipid solution. When droplets containing the Alm biomolecules are connected to neighboring droplets, Alm inserts itself into the membrane and assembles a conductive voltage-gated pore.

The current was supplied and measured by an Axopatch 200B (Molecular Devices), connected to an arbitrary function generator (Agilent, 33220A), and acquired through a Digidata 1440A (Molecular Devices). Measurements are taken on a vibration isolation stage (Vision IsoStation, Newport), and the experiment is performed under a fixed-stage brightfield microscope (Zeiss Axioskop). Pictures are taken through an attached axiocam (Zeiss).

Electrodes were created using a 40% weight/volume PEG-DMA hydrogel (Polysciences, Inc.), combined with Irgacure (O-BASF) and a 500 mM KCl solution (Sigma Aldrich) with 10 mM MOPS pH buffer (Sigma Aldrich). 1 mm borosilicate glass capillary tubes (World Precision Instruments) were filled with this hydrogel solution using 34 G microfils (World Precision Instruments), and silver/silver-chloride (Ag/AgCl) electrodes were embedded inside the uncured hydrogel. The hydrogel was then cured with a UV light emitting diode (LED), fixing the Ag/AgCl electrodes into place. Droplets of the liposome-containing aqueous solution may then be suspended from the extruded hydrogel at the tip of the capillary tubes attached to the micromanipulators within the oil reservoir, allowing for mechanically controllable droplets with embedded electrodes for electrical measurements.

[1]S. Sarles and D. Leo, "Membrane-based biomolecular smart materials," Smart Mater. Struct. **20**, 094018 (2011).
[2]J. Xu, F. J. Sigworth, and D. A. LaVan, "Synthetic protocells to mimic and test cell function," Adv. Mater. **22**(1), 120–127 (2010).
[3]R. Keynes and H. Martins–Ferreira, "Membrane potentials in the electroplates of the electric eel," J. Physiol. **119**(2–3), 315–351 (1953).
[4]D. Bray, "Intracellular signalling as a parallel distributed process," J. Theor. Biol. **143**(2), 215–231 (1990).
[5]L. H. Hartwell, J. J. Hopfield, S. Leibler, and A. W. Murray, "From molecular to modular cell biology," Nature **402**(6761), C47–C52 (1999).
[6]H. Bayley, B. Cronin, A. Heron, W. L. Hwang, R. Syeda, J. Thompson, and M. Wallace, "Droplet interface bilayers," Mol. Biosyst. **4**(12), 1191–1208 (2008).
[7]M. A. Holden, D. Needham, and H. Bayley, "Functional bionetworks from nanoliter water droplets," J. Am. Chem. Soc. **129**(27), 8650–8655 (2007).
[8]G. Villar, A. D. Graham, and H. Bayley, "A tissue-like printed material," Science **340**(6128), 48–52 (2013).
[9]K. Funakoshi, H. Suzuki, and S. Takeuchi, "Lipid bilayer formation by contacting monolayers in a microfluidic device for membrane protein analysis," Anal. Chem. **78**(24), 8169–8174 (2006).
[10]Y. Elani, X. Niu, and O. Ces, "Novel technologies for the formation of 2-D and 3-D droplet interface bilayer networks," Lab Chip **12**(18), 3514–3520 (2012).
[11]P. Carreras, R. Law, N. Brooks, J. Seddon, and O. Ces, "Microfluidic generation of droplet interface bilayer networks incorporating real-time size sorting in linear and non-linear configurations," Biomicrofluidics **8**(5), 054113 (2014).
[12]G. J. Taylor and S. A. Sarles, "Heating-enabled formation of droplet interface bilayers using *Escherichia coli* total lipid extract," Langmuir **31**, 325–337 (2015).
[13]N. Tamaddoni, E. C. Freeman, and S. A. Sarles, "Sensitivity and directionality of lipid bilayer mechanotransduction studied using a revised, highly durable membrane-based hair cell sensor," Smart Mater. Struct. **24**(6), 065014 (2015).

[14]G. J. Taylor, G. Venkatesan, P. Collier, and S. A. Sarles, "Direct *in situ* measurement of specific capacitance, monolayer tension, and bilayer tension in a droplet interface bilayer," Soft Matter **11**(38), 7592–7605 (2015).
[15]J. B. Boreyko, G. Polizos, P. G. Datskos, S. A. Sarles, and C. P. Collier, "Air-stable droplet interface bilayers on oil-infused surfaces," Proc. Natl. Acad. Sci. **111**(21), 7588–7593 (2014).
[16]G. Maglia, A. J. Heron, W. L. Hwang, M. A. Holden, E. Mikhailova, Q. Li, S. Cheley, and H. Bayley, "Droplet networks with incorporated protein diodes show collective properties," Nat. Nanotechnol. **4**(7), 437–440 (2009).
[17]M. A. Creasy, E. C. Freeman, M. K. Philen, and D. J. Leo, "Deterministic model of biomolecular networks with stimuli-responsive properties," J. Intell. Mater. Syst. Struct. **26**, 921–930 (2014).
[18]W. L. Hwang, M. A. Holden, S. White, and H. Bayley, "Electrical behavior of droplet interface bilayer networks: experimental analysis and modeling," J. Am. Chem. Soc. **129**(38), 11854–11864 (2007).
[19]S. I. Sukharev, P. Blount, B. Martinac, F. R. Blattner, and C. Kung, "A large-conductance mechanosensitive channel in E. coli encoded by mscL alone," Nature **368**(6468), 265–268 (1994).
[20]F. Bezanilla, "Voltage-gated ion channels," IEEE Trans. Nanobiosci. **4**(1), 34–48 (2005).
[21]J. Allen, "Photosynthesis of ATP-electrons, proton pumps, rotors, and poise," Cell **110**, 273–276 (2002).
[22]F. Hucho and C. Weise, "Ligand-gated ion channels," Angew. Chem. Int. Ed. **40**(17), 3100–3116 (2001).
[23]M. S. P. Sansom, "Alamethicin and related peptaibols—Model ion channels," Eur. Biophys. J. **22**(2), 105–124 (1993).
[24]D. P. Tieleman, B. Hess, and M. S. P. Sansom, "Analysis and evaluation of channel models: Simulations of alamethicin," Biophys. J. **83**(5), 2393–2407 (2002).
[25]P. Yang, F. G. Wu, and Z. Chen, "Dependence of alamethicin membrane orientation on the solution concentration," J. Phys. Chem. C **117**(7), 3358–3365 (2013).
[26]G. A. Woolley and B. A. Wallace, "Model ion channels—Gramicidin and alamethicin," J. Membr. Biol. **129**(2), 109–136 (1992).
[27]D. P. Tieleman, M. S. P. Sansom, and H. J. C. Berendsen, "Alamethicin helices in a bilayer and in solution: Molecular dynamics simulations," Biophys. J. **76**(1), 40–49 (1999).
[28]P. C. Biggin, J. Breed, H. S. Son, and M. S. P. Sansom, "Simulation studies of alamethicin-bilayer interactions," Biophys. J. **72**(2), 627–636 (1997).
[29]S. L. Keller, S. M. Bezrukov, S. M. Gruner, M. W. Tate, I. Vodyanoy, and V. A. Parsegian, "Probability of alamethicin conductance states varies with nonlamellar tendency of bilayer phospholipids," Biophys. J. **65**(1), 23–27 (1993).
[30]P. La Rocca, P. C. Biggin, D. P. Tieleman, and M. S. P. Sansom, "Simulation studies of the interaction of antimicrobial peptides and lipid bilayers," Biochim. Biophys. Acta, Biomembr. **1462**(1–2), 185–200 (1999).
[31]K. He, S. J. Ludtke, W. T. Heller, and H. W. Huang, "Mechanism of alamethicin insertion into lipid bilayers," Biophys. J. **71**(5), 2669–2679 (1996).
[32]R. Nagaraj and P. Balaram, "Alamethicin, a transmembrane channel," Acc. Chem. Res. **14**(11), 356–362 (1981).
[33]R. O. Fox and F. M. Richards, "A voltage-gated ion channel model inferred from the crystal-structure of alamethicin at 1.5-A resolution," Nature **300**(5890), 325–330 (1982).
[34]D. P. Tieleman, H. J. C. Berendsen, and M. S. P. Sansom, "An alamethicin channel in a lipid bilayer: Molecular dynamics simulations," Biophys. J. **76**(4), 1757–1769 (1999).
[35]D. P. Tieleman, H. J. C. Berendsen, and M. S. P. Sansom, "Voltage-dependent insertion of alamethicin at phospholipid/water and octane/water interfaces," Biophys. J. **80**(1), 331–346 (2001).
[36]D. P. Tieleman, L. R. Forrest, M. S. P. Sansom, and H. J. C. Berendsen, "Lipid properties and the orientation of aromatic residues in OmpF, influenza M2, and alamethicin systems: Molecular dynamics simulations," Biochemistry **37**(50), 17554–17561 (1998).
[37]B. Hess, C. Kutzner, D. van der Spoel, and E. Lindahl, "Gromacs 4: Algorithms for highly efficient, load–balanced, and scalable molecular simulation," J. Chem. Theory Comput. **4**(3), 435–447 (2008).
[38]A. D. MacKerell, D. Bashford, M. Bellott, R. L. Dunbrack, J. D. Evanseck, M. J. Field, S. Fischer, J. Gao, H. Guo, S. Ha, D. Joseph-McCarthy, L. Kuchnir, K. Kuczera, F. T. K. Lau, C. Mattos, S. Michnick, T. Ngo, D. T. Nguyen, B. Prodhom, W. E. Reiher, B. Roux, M. Schlenkrich, J. C. Smith, R. Stote, J. Straub, M. Watanabe, J. Wiorkiewicz-Kuczera, D. Yin, and M. Karplus, "All-atom empirical potential for molecular modeling and dynamics studies of proteins," J. Phys. Chem. B **102**(18), 3586–3616 (1998).
[39]D. J. Evans and B. L. Holian, "The Nose-Hoover thermostat," J. Chem. Phys. **83**(8), 4069–4074 (1985).
[40]O. S. Smart, J. G. Neduvelil, X. Wang, B. A. Wallace, and M. S. P. Sansom, "HOLE: A program for the analysis of the pore dimensions of ion channel structural models," J. Mol. Graphics Modell. **14**(6), 354 (1996).
[41]D. B. Wells, M. Belkin, J. Comer, and A. Aksimentiev, "Assessing graphene nanopores for sequencing DNA," Nano Lett. **12**(8), 4117–4123 (2012).
[42]L. M. Harriss, B. Cronin, J. R. Thompson, and M. I. Wallace, "Imaging multiple conductance states in an alamethicin pore," J. Am. Chem. Soc. **133**(37), 14507–14509 (2011).
[43]S. Senapati and A. Chandra, "Dielectric constant of water confined in a nanocavity," J. Phys. Chem. B **105**(22), 5106–5109 (2001).
[44]J. O. M. Bockris, A. K. N. Reddy, and M. E. Gamboa-Aldeco, *Modern Electrochemistry* (Plenum Press, New York, 1998).
[45]J. Newman and K. E. Thomas-Alyea, *Electrochemical Systems* (Wiley-Interscience, 2012).
[46]E. Samson, J. Marchand, and K. Snyder, "Calculation of ionic diffusion coefficients on the basis of migration test results," Mater. Struct. **36**(3), 156–165 (2003).
[47]O. S. Andersen, A. Finkelstein, I. Katz, and A. Cass, "Effect of phloretin on the permeability of thin lipid membranes," J. Gen. Physiol. **67**(6), 749–771 (1976).
[48]L. Wang, "Measurements and implications of the membrane dipole potential," Annu. Rev. Biochem. **81**, 615–635 (2012).
[49]M. A. Creasy, *Bilayer Network Modeling* (Virginia Polytechnic Institute and State University, 2011).
[50]V. B. Sundaresan and D. J. Leo, "Modeling and characterization of a chemomechanical actuator using protein transporter," Sens. Actuators, B **131**(2), 384–393 (2008).
[51]M. Ohno, T. Hamada, K. Takiguchi, and M. Homma, "Dynamic behavior of giant liposomes at desired osmotic pressures," Langmuir **25**(19), 11680–11685 (2009).

[52]S. S. Dixit, A. Pincus, B. Guo, and G. W. Faris, "Droplet shape analysis and permeability studies in droplet lipid bilayers," Langmuir **28**(19), 7442–7451 (2012).
[53]H. O. Negrete, R. L. Rivers, A. H. Gough, M. Colombini, and M. L. Zeidel, "Individual leaflets of a membrane bilayer can independently regulate permeability," J. Biol. Chem. **271**(20), 11627–11630 (1996).
[54]L. Endresen, K. Hall, J. Høye, and J. Myrheim, "A theory for the membrane potential of living cells," Eur. Biophys. J. **29**(2), 90–103 (2000).
[55]E. Guggenheim, "The conceptions of electrical potential difference between two phases and the individual activities of ions," J. Phys. Chem. **33**(6), 842–849 (1928).
[56]A. C. Hindmarsh, P. N. Brown, K. E. Grant, S. L. Lee, R. Serban, D. E. Shumaker, and C. S. Woodward, "SUNDIALS: Suite of nonlinear and differential/algebraic equation solvers," ACM Trans. Math. Software **31**(3), 363–396 (2005).
[57]J. Andersson, J. Åkesson, and M. Diehl, "CasADi: A symbolic package for automatic differentiation and optimal control," in *Recent Advances in Algorithmic Differentiation* (Springer, 2012), pp. 297–307.
[58]W. Hanke and G. Boheim, "The lowest conductance state of the alamethicin pore," Biochim. Biophys. Acta, Biomembr. **596**(3), 456–462 (1980).
[59]E. C. Freeman, M. K. Philen, and D. J. Leo, "Using cellular energy conversion and storage mechanics for bio-inspired energy harvesting," Proc. SPIE **8686**, 868613 (2013).
[60]A. Kancharala, E. Freeman, and M. Philen, "Energy harvesting from droplet interface bilayers," in *ASME 2015 Conference on Smart Materials, Adaptive Structures and Intelligent Systems* (American Society of Mechanical Engineers, 2015).
[61]E. Freeman and L. Weiland, "Biologically inspired reversible osmotic actuation through voltage-gated ion channels," J. Intell. Mater. Syst. Struct. **23**(12), 1395–1403 (2012).